Sustainable Energy Technologies and Assessments xxx (xxxx) xxx

Contents lists available at ScienceDirect

Sustainable Energy Technologies and Assessments

journal homepage: www.elsevier.com/locate/seta

A numerical study on frosting and its early stage under forced convection conditions with surface and environmental factors considered

Lei Shangwen[a], Song Mengjie[a,b,*], Pekař Libor[c], Shen Jun[d]

[a] Department of Energy and Power Engineering, School of Mechanical Engineering, Beijing Institute of Technology, 100081 Beijing, China
[b] School of Environment & Architecture, University of Shanghai for Science & Technology, No. 516, Jungong Road, Shanghai, China
[c] Department of Automation and Control Engineering, Faculty of Applied Informatics, Tomas Bata University in Zlín, Nad Stráněmi 4511, 76005 Zlín, Czech Republic
[d] Key Laboratory of Cryogenics, Technical Institute of Physics and Chemistry, Chinese Academy of Sciences, Beijing 100190, China

ARTICLE INFO

Keywords:
Early frosting stage
Forced convection
Surface wettability and environmental factors
Sensitivity analysis
Model optimization

ABSTRACT

To accurately control the frosting process, analyzing the influence of different factors on frosting is meaningful and challengeable, especially in the early frosting stage. According to the sensitivity analysis, the influence of different surface wettability and environmental factors on the growth of frost layer were quantitatively analyzed. Based on the experimental data on cold plate surface under forced convection conditions, new models with emphasis on the initial conditions of the frosting process are developed. Results show that supersaturation degree, supercooling degree and cold plate temperature are the key factors on the growth of frost layer, but their specific influence varies in the early frosting stage. And proportions of these three factors reach 39.42%, 35.58% and 21.15%, respectively. The coincidence rates of the new models with an error of 15% reach>90% for the whole frosting process, and 83% for the early frosting stage. Compared with previous models, the coincidence rates of the new models for the whole frosting process and the early frosting stage are increased by at least 8.86% and 15.28%, respectively. Contributions of this study are expected to predict the growth of frost layer in the early frosting stage and provide a reference for the optimal defrosting control of air source heat pumps.

Introduction

Frost deposition is inevitable once moist air is exposed to a cold surface, whose temperature is below the water triple point and the air dew point [1]. For a heat exchanger, after frost accumulated and a continuous frost layer formed, the heat transfer resistance will dramatically increase [2]. For an air source heat pump, the coefficient of performance decreases due to the increasing frost layer, or even an unexpected system malfunction [3,4]. To solve the frosting problem, the heat transfer systems have to allocate more energy to defrost by using mechanical or thermal methods [5,6]. That means, the control system would become more complicated and more time consumed due to the defrosting operation [7]. To avoid these drawbacks, accurately predict or control the frosting process becomes necessary. Because the frosting process is influenced by many factors, around the cold plate surface and environmental air conditions [8], analyzing the key influencing factors in the frosting process is meaningful and challengeable.

The factors mostly analyzed in open literatures include surface wettability, surface roughness, surface temperature, air velocity, air temperature and air relative humidity [9]. For example, the influence of surface wettability was investigated by Wang et al. [10] in an experimental study. As reported, on a hydrophobic surface at a contact angle of 147°, frost nucleation was delayed by nearly 60 min. For the factor of surface roughness, it is experimentally investigated and quantitively analyzed by Hermes et al. [8]. When the roughness value is higher, it's found that more nucleation sites are generated on the surface. It is easy to understand the water content in surrounding air of cold plate is the source of frost. The experimental results reported by Amer and Wang [11] show that increasing the relative humidity will not only increase the frost thickness, but also affect the frost property, such as its density or thermal conductivity coefficient. The influence of surface and air temperature on frosting process were investigated by Lüer and Beer [12]. As reported, surface temperature strongly affects the average frost thickness and the density. While, after the air relative humidity was fixed or water content in air was constant, the variation of air temperature shows minor effect on frost formation. Seeing from the micro view [13,14], higher air velocity would accelerate the change of frost crystals

* Corresponding author at: Department of Energy and Power Engineering, School of Mechanical Engineering, Beijing Institute of Technology, 100081 Beijing, China.
E-mail addresses: mengjie.song@gmail.com, mengjie.song@bit.edu.cn (M. Song).

https://doi.org/10.1016/j.seta.2021.101202
Received 12 December 2020; Received in revised form 6 March 2021; Accepted 21 March 2021

Nomenclatures

Variable	Description (Unit)
a	slope (mm $s^{-1/2}$)
b	intercept (mm $s^{1/2}$)
c_p	specific heat (kJ kg^{-1} K^{-1})
D	diffusivity of vapor in air (m^2 s^{-1})
h_m	coefficient of mass transfer (m s^{-1})
i_{sv}	latent heat of sublimation (kJ kg^{-1})
Ja	modified Jakob number (/)
k	thermal conductivity (W m^{-1} K^{-1})
L	cold plate length (m)
M	mass flux (kg m^{-2} s^{-1})
Pr	Prandtl number (/)
q	heat flux (W m^{-2})
Re	Reynolds number (/)
RH	relative humidity of air (/)
T	temperature (K)
t	time (s)
V	air velocity (m s^{-1})
Cr	coincidence rate (/)

Greek symbols

δ	frost thickness (m)
θ	contact angel (degree)
ρ	density (kg m^{-3})
ω	absolute humidity of air ($g_v g_a^{-1}$)
Δ	relative error deviation (/)

Subscripts

a	air (/)
dp	dewpoint (/)
f	frost (/)
i	ice (/)
s	solid (/)
sat	saturation (/)
v	vapor (/)
w	wall (/)

from feather crystals to irregular crystals and made frost crystals appear close to each other [15]. Although frosting on cold plates is more fundamental and commonly reported [16,17], other shapes of frosting surface were also studied, such as round tube [18,19], fin bases [20], parallel plates [21], etc. The surface shape directly affects the parameters of surrounding air, and thus may affect the frosting process. It can be seen that there are many factors influencing the frosting process, and their influence vary from each factor. However, most of the existing literature only take a few factors to illustrate the frosting process. The reason is, under the unified investigation of multiple factors, there are secondary factors having minor effect on the frosting process, but significantly increase the experimental and analytical work [9]. Therefore, it is necessary to find out the key influence factors on the frosting process with multiple factors considered, so as to effectively reflect the frosting process.

However, the same factors on the frosting process may also be different. For example, hydrophobic surface is widely reported in delaying frosting [22,23], and frost nucleation becomes more difficult as the surface contact angle increases [24]. But it is reported by Sommers et al. [25] that the surface energy, with surface contact angle included, shows a wake influence on frosting process. It is generally reported that the increase of air velocity would increase the frost thickness. But the frost thickness is independent of the air velocity as reported by Lee and Lee [26]. The different influence of a fixed factor may result from it working in different frosting stages. As shown in Fig. 1, based on the four periods divided by Song and Dang [9], an entire frosting process could be further divided into four stages. In the no frost stage, the droplet nucleation occurs first, as well as the coalescence of the droplets occurred immediately after the nucleation. As the phase change occurs, the droplets merge and solidify, and their diameters and heights increase significantly. After reaching the critical time, t_c, all coalescent droplets turned into ice particles or crystals. In the early stage, non-uniform tip growth occurs on individual crystals. After that, frost branches would form at the top of the crystals. These frost branches grew in three dimensions and connected to neighboring frost branches, thus forming a flat frost layer. In the middle stage, the frost layer appears globally homogenous and possesses characteristics of a porous medium with its height increases steadily. In the final stage, because the periodic frosting and defrosting process caused by the fluctuation of the thermal resistance of the porous frost layer occurs, the height of the frost layer keeps constant. It is obvious for the surface wettability effect on the no frost stage, while the effect disappears at latter three stages [27,28]. Compared with the latter two stages, the early stage takes shorter time in a frosting duration. At this stage, higher wind speed will promote the convective heat transfer between the frost surface and the environment, thus has a certain influence on the frost thickness. While in the latter two stages, the increase of air velocity is helpful to the nucleation of the moist air in the porous frost layer, thus has an obvious effect on the frost density [7,29]. Therefore, when analyzing the influence of a fixed factor on frosting process, difference of stages should also be considered.

To illustrate the frost properties in the frosting process, many frosting models were proposed in the open literature [25,30–34]. However, these frosting models based on the whole frosting process actually only considered the middle and final frosting stages, and didn't pay much attention to the early frosting stage. For example, A new semi-empirical correlation for frost thickness proposed by Sommers et al. [25] was reported with an average predictive error of 11.7% for nearly 930 experimental data points. But the authors clearly pointed out that the model was not suitable for the initial conditions of frosting. Although the model proposed by Hermes et al. [30] predicted well the experimental trends for frost thickness for the time over 30 min, it showed poor comparisons at the early stage. And same poor predictions happened on

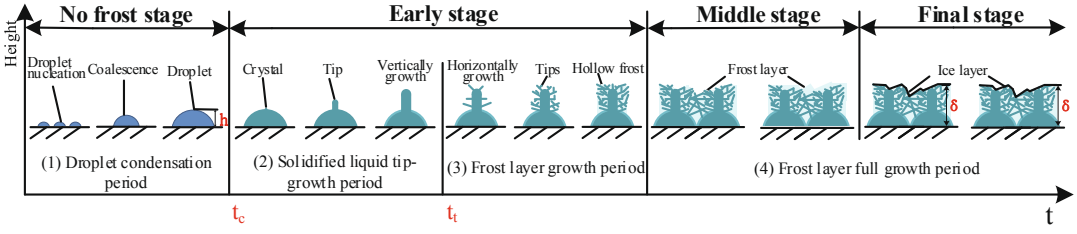

Fig. 1. Early frosting stage in an entire frosting process.

his previous model, too [31]. By using a computational fluid dynamics-based model developed by Kim et al. [32], the average frost density was in good agreement with experimental data with an error of 10% after 60 min. But during the early frosting stage, the maximum error reached 25%. In the study reported by Negrelli and Hermes [33], comparisons of the proposed correlation with the experimental data showed that only 81% of the data points with an error of 15% could be predicted. And it may result from ignoring of the early frosting stage. In the study of Zendehboudi and Hosseini [34], regression plots between the measured values and the actual values of frost layer thickness forecasted by six different approaches were presented. But still, five of the six approaches had obvious regression deviation in fitting of the initial conditions of frosting. Actually, during the early frosting stage, the rapid changes of frost properties make the analysis become more difficult [35]. And the uneven distribution of frost layer makes the frost thickness hard to be experimentally measured [29]. Many numerical studies are thus seriously distorted when reflecting the early frosting process. Therefore, to improve the validation accuracy of frosting numerical models, the early frosting stage should be specially considered.

To sum up, influence of different factors on frosting process varies, while many existing studies investigate several factors at a time with incomprehensive results [36]. So, simultaneously investigate the multi factors becomes necessary. But as some secondary factors have minor effect on frosting, finding out the key influence factors by sensitivity analysis is helpful to the analysis of the frosting process [37,38]. On the other hand, the influence of factors in each frosting stage may be different. Many studies have focused on the middle and final frosting stages, with the early frosting stage not specially mentioned. This results in low accuracy of the numerical models reported. Therefore, to accurately predict and control the frosting process, it is of great significance to develop a frosting model and analyze the key factors, with the early frosting stage specially considered. Firstly, based on the reported experimental data on cold plate under forced convection conditions, sensitivity analysis with surface and environmental factors considered is carried out. Then, in the modeling process, the influence of the key factors on frosting in the initial conditions of frosting is specially considered, and the corresponding frosting models are developed. After analyzing and discussing the differences between the key factors in the early frosting stage, the new models are further compared with previous models and validated with experimental data from different studies. Finally, quantitative conclusions of predicting frost growth are given.

Methods

Theoretical model of frost layer thickness

The theoretical model of frost thickness relies on the following assumptions: (i) quasistatic, one-dimensional mass and heat diffusion, (ii) uniform frost layer along the flat plate, and (iii) the applicability of the Lewis analogy [39]. Therefore, both processes of frost growth and densification are represented by the mass balance on and within the frost layer, and thus the total mass flux of water vapor transferred toward the frost layer is given by

$$M = \frac{d}{dt}\left(\delta \cdot \rho_f\right) = \delta \frac{d\rho_f}{dt} + \rho_f \frac{d\delta}{dt} \tag{1}$$

where, t is the frosting duration, δ is the frost thickness, ρ_f is the density of frost layer, and M is the mass flux. The first term of Eq. (1) refers to the process of frost layer densifying over time, and the second term represents the part of water vapor increasing the frost thickness. On the other hand, the frosting process follows the energy conservation theory. The total energy transferred to the frost layer includes the convection heat transfer on the frost layer and the latent heat of solidification released by the vapor within the entire frost layer. Based on the energy conservation theory, ρ_f was simplified by Hermes et al. [40] and could be calculated by a semi-empirical correlation covering a wide range of operating conditions with an error of 15%.

$$\frac{\rho_f}{\rho_i} = CJa^{-n}\sqrt{t} \tag{2}$$

where, ρ_i is the density of the ice, C is a constant or a function of the contact angle and the relative humidity, and n is a constant. Ja represents the ratio between the sensible heat and latent heat involved in the desublimation process, and which could be calculated as follows.

$$J_a = \left(c_p / i_{sv}\right)\left(T_{dp} - T_w\right) / \left(\omega - \omega_{sat,w}\right) \tag{3}$$

where, c_p is the specific heat of the air, and i_{sv} is the latent heat of sublimation. T_{dp} and T_w are the dew temperature of the moist air and the temperature of the cold plate, respectively. The absolute humidity of the air and the absolute humidity of the saturated air at the temperature of the cooled surface correspond to ω and $\omega_{sat,w}$, respectively. So, substituting Eqs. (2) and (3) into Eq. (1), the frost thickness could be obtained,

$$\delta(t) = \left(\frac{M}{\rho_i CJa^{-n}}\right)\sqrt{t} + \frac{b}{\sqrt{t}} \tag{4}$$

where, b is a constant, and M could be calculated as follows.

$$M = h_m \rho_a \left(\omega_a - \omega_{sat,w}\right) \tag{5}$$

where, ω_a is the absolute humidity of the air, h_m is the convective mass transfer coefficient. Based on the Lewis analogy [39,8], h_m could be calculated as follows.

$$h_m = (D/L)Re^m Pr^{1/3} \tag{6}$$

where, D is the diffusivity of the water vapor in air, L is the length of the plate, Re is the Reynolds number, Pr is the Prandtl number, and m corresponds to a constant, and is nearly 1/2 for laminar and 4/5 for turbulent flows. Therefore, the basic expression of frost thickness can be rearranged as follows.

$$\delta(t) = c\left(\frac{\rho_a}{\rho_i}\right)\left(\frac{D\Delta\omega}{L}\right)Re^m Pr^{1/3} Ja^n \sqrt{t} + \frac{b}{\sqrt{t}} \tag{7}$$

where, $\Delta\omega/L$ is the humidity gradient, which could be short for Eq. (8) as shown below. And $\Delta\omega$ is named the supersaturation degree, representing the humidity ratio difference between the air stream and the frosting surface.

$$\Delta\omega/L = \left(\omega_a - \omega_{sat,w}\right)/L \tag{8}$$

In Eq. (7), two asymptotes lie in the time domain, one related to the first term $\sqrt{t}$ and the other related to the second term $1/\sqrt{t}$. With the increase of t, the values of the first and second terms will increase and decrease, respectively. So, the first term stands for the frost growth over time, while the second represents descent of the frost decay. To illustrate the variation of frost thickness with time, take the derivative of δ to t, as shown below.

$$\frac{d\delta}{dt} = \left[\frac{1}{2}c\left(\frac{\rho_a}{\rho_i}\right)\left(\frac{D\Delta\omega}{L}\right)Re^m Pr^{1/3} Ja^n - \frac{b}{2t}\right]\frac{1}{\sqrt{t}} \tag{9}$$

In Eq. (9), the first and second terms in the bracket are positive, and the two terms are subtracted. However, at the beginning of frosting, i.e. $t = 0^+$, the second term is much larger than the first term, which makes the difference in the bracket negative. Define $t = t_1$ as the time at the zero point of the deviation, thus when the time is less than t_1, the derivative of Eq. (7) is negative. Moreover, when the value of t is less than 1, the negative value is greatly amplified by $1/\sqrt{t}$, and then gradually decreases during $1 \sim t_1$. Therefore, when the time is less than t_1, the derivative of Eq. (7) is negative and the variation of the derivative is

large. Then the frost layer thickness decreases rapidly with time, as shown by the green dotted line in Fig. 2. When the time reaches t_1 and the derivative of Eq. (7) is 0, the frost thickness reaches the minimum value. After the time exceeds t_1, the derivative of Eq. (7) gets positive and the variation of derivative tends to be gentle. Then the frost layer thickness increases steadily with time. When frosting enters the final frosting stage, the frost thickness will remain constant due to periodic frosting and defrosting process, as shown by the red solid line.

However, the mass flux of frost layer won't be negative during the whole frosting process, so the growth of frost layer represented by green dotted line is impossible. As shown in Fig. 1, the early frost layer will continue to grow on the frozen water droplet embryo formed in the no frost stage, and the growth rate of the frost layer along the vertical direction is fast in the early frosting stage. So, from the time duration of 0 to t_1, the growth of the frost layer becomes an upward convex curve, as shown in the blue solid line in Fig. 2. When the time reaches t_1, the slope of the blue line reaches 0, thus realizing the connection with the red line. It should be noted that the duration of 0 to t_1 is short when compared with the latter durations, and the growth of frost layer is actually like the early frosting stage. That is, the growth of frost layer in the period from 0 to t_1 reflects the variation trend of frost thickness with time in the early frosting stage. Afterwards, the frosting performance corresponds to the variation trend of frost layer in the middle and final frosting stages.

Theoretical basis of optimization

In Eq. (7), the first term stands for the frost growth over time, while the second is associated with frost decay. Eq. (7) can be simplified as follows.

$$\delta = a\sqrt{t} + b/\sqrt{t} \tag{10}$$

or,

$$\delta\sqrt{t} = at + b \tag{11}$$

From the expression of Eq. (11), t and $\delta\sqrt{t}$ could be regarded as the independent and dependent variables of a linear equation, respectively. Therefore, the slope of the linear equation is a, which represents the growth rate of frost thickness over time during the whole frosting process. And the intercept of the linear equation is b, which represents the initial conditions of the frosting process, that is, the early frosting stage. Considering the dependence of the frost thickness with the surface wettability, the b-coefficient of Eq. (7) is expressed as an exponential function of contact angle by Hermes et al. [8] as follows.

$$b = de^{k\theta} \tag{12}$$

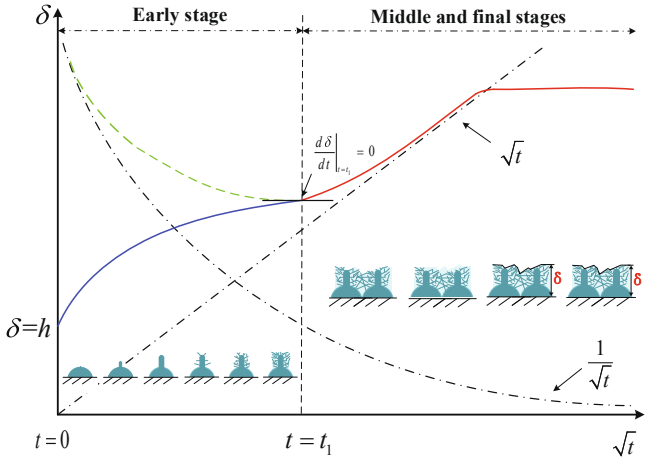

Fig. 2. The variation trend of frost thickness with time at three frosting stages.

where, d and k are constants, and θ is the contact angle. Therefore, the theoretical model proposed by Hermes et al. [8] could be rearranged as follows.

$$\delta(t) = c\left(\frac{\rho_a}{\rho_i}\right)\left(\frac{D\Delta w}{L}\right)Re^m Pr^{1/3} Ja^n\sqrt{t} + \frac{de^{k\theta}}{\sqrt{t}} \tag{13}$$

In such a way the coefficients c, d, m, n and k of this theoretical model are to be fitted against the experimental data. Results show that most of the experimental points lie in the error of 15%, with 131 points out of 792 outside of this range. That is, the theoretical model is able to predict 83% of the experimental data points. Now define the relationship between δ, A and B as shown in Eqs. (14) and (15) below.

$$\delta(t) = c\left(\frac{\rho_a}{\rho_i}\right)\left(\frac{D\Delta w}{L}\right)Re^m Pr^{1/3} Ja^n\sqrt{t} + \frac{de^{k\theta}}{\sqrt{t}} = A + B \tag{14}$$

$$A = c\left(\frac{\rho_a}{\rho_i}\right)\left(\frac{D\Delta \omega}{L}\right)Re^m Pr^{1/3} Ja^n\sqrt{t}B = \frac{de^{k\theta}}{\sqrt{t}} \tag{15}$$

From the content of analogy, A and B correspond to a and b of Eq. (11), respectively. Therefore, A/δ and B/δ reflect the proportions of the whole frosting process and the early frosting stage in the expression of frost thickness, respectively. Because the influence of various factors on frosting in each stage is different, the proportions of A/δ and B/δ are changing within the whole frosting process. To clearly show the difference of fitting of A/δ and B/δ when reflecting the frosting process, the experimental data of a 7,200 s-experiment obtained by Hermes et al. [8] is used in this study. Divide 7,200 s into several periods, as shown in Table 1. It should be noted that in the process of fitting, the coincidence rate (Cr) represents the ratio between the fitted and experimental frost thickness data points with the relative error deviation (Δ) of 15%. And the relative error deviation (Δ) could be calculated as follows.

$$\Delta = \frac{\delta_{\text{fit}} - \delta}{\delta} \tag{16}$$

where, δ_{fit} is the fitted frost thickness obtained by the fitting correlation.

Table 1
Summary of the fitting results of the theoretical model in each period.

Group	Period (s)	Coincidence number/ Total number	Cr (%)	A/δ (%)	B/δ (%)
1	600–7,200	579/715	83.00	>99	<1
2	600–1,200	93/130	71.53	>99	<1
	2,400–3,000	118/130	90.76	98 ~ 99	1 ~ 2
	3,600–4,200	118/130	90.76	82 ~ 93	7 ~ 18
	4,800–5,400	119/130	91.53	70 ~ 87	13 ~ 30
	6,000–7,200	175/195	91.79	67 ~ 86	14 ~ 33
	600–7,200	627/715	87.69	/	/
3	600–2,400	151/195	77.43	>99	<1
	3,000–4,200	177/195	90.76	90 ~ 96	4 ~ 10
	4,800–6,000	179/195	91.79	72 ~ 88	12 ~ 28
	6,600–7,200	122/130	93.84	65 ~ 83	17 ~ 35
	600–7,200	628/715	87.83	/	/
4	600–3,000	212/260	81.53	>99	<1
	3,600–5,400	237/260	91.15	79 ~ 93	7 ~ 21
	6,000–7,200	179/195	91.79	67 ~ 86	14 ~ 33
	600–7,200	628/715	87.83	/	/
5	600	48/65	73.84	>99	<1
	1,200	51/65	78.46	>99	<1
	2,400	60/65	92.30	97 ~ 99	1 ~ 3

As shown in Table 1, compared with $Cr = 83\%$ in Group 1 obtained by the theoretical model [8] within 7,200 s, that of the staged fitting at least increases to 87.69%, which means the staged fitting can indeed improve the fitting effect. However, the improvement of the staged fitting is not obvious. In the observation of the fitting effect of each group, *Cr* of the periods within 2,400 s is significantly lower than that of other periods. As shown in Groups 2–4, *Crs* of the periods within 600–1,200, 600–2,400 and 600–3,000 are 71.53%, 77.43% and 81.53%, respectively, while *Crs* of other periods are at least 90%. In Group 5, the experimental data of 600, 1,200 and 2,400 s are separately fitted with Eq. (13), it can be seen that *Crs* are obviously lower within 1,200 s.

The reason of the poor fitting effect of the model is that this model can't express the relationship between the experimental data and the model expression. Therefore, Eq. (13) as the early frosting stage model is not ideal. As mentioned earlier, B/δ reflects the proportion of the early frosting stage in the expression of frost thickness. As shown in Table 1, B/δ is at least greater than 1% in most periods and *Crs* of these periods are greater than 90%, indicating a good fitting effect. However, B/δ in periods within 1,200 s with poor fitting effect is less than 1%, which means Eq. (13) doesn't express the performance of frost growth in early frosting stage. To reflect the proportion of the early frosting stage, the emphasis should be put on the reflection of B/δ.

Sensitivity analysis

The model optimization process needs to investigate the influence degree of each variable on frosting, so sensitivity analysis is needed. As a indicates the frost growth rate and b informs the initial conditions of the frosting process, by investigating the influence of factors on a and b, the key factors in the frosting process can be found. In this section, multivariate linear fitting is introduced to investigate the linear relationship between the independent variables and the dependent variables, as shown below.

$$\widehat{a} = \alpha_0 + \alpha_1 \Delta\widehat{\omega} + \alpha_2 \Delta\widehat{T} + \alpha_3 \widehat{V} + \alpha_4 \widehat{T}_w + \alpha_5 \widehat{T}_a + \alpha_6 \widehat{\theta} \tag{17}$$

$$\widehat{b} = \beta_0 + \beta_1 \Delta\widehat{\omega} + \beta_2 \Delta\widehat{T} + \beta_3 \widehat{V} + \beta_4 \widehat{T}_w + \beta_5 \widehat{T}_a + \beta_6 \widehat{\theta} \tag{18}$$

where ΔT is the supercooling degree, representing the temperature difference between the frost surface and the dew-point. The coefficients belonged to the independent variables directly reflect the influence of independent variables on the dependent variable. By summing up the absolute values of each coefficient, the proportion of the absolute value of a single coefficient in the sum can be obtained. Then the independent variables having obvious influence on the dependent variable will be found. In all cases, dimensionless forms of the independent and dependent variables were adopted, being calculated from,

$$\widehat{y} = \frac{y - \frac{y_{max}+y_{min}}{2}}{\frac{y_{max}-y_{min}}{2}} \tag{19}$$

Use the experimental data of 69 groups obtained by the frost growth on a cold plate under forced convection conditions provided by Hermes et al. [8], through simple linear fitting of Eq. (11), the corresponding a and b of each group can be obtained. Afterwards, a rich set of a and b arrays which can be used for sensitivity analysis will be set up, so as to investigate the influence of each independent variable on the dependent variables. Take the Test #16 as a sample, as shown in Fig. 3. The slope of the dotted line represents the value of a, so $a = 0.0392$. The intercept of the dotted line on the y-axis represents the value of b, so $b = 0.11$. Moreover, the goodness of the linear fitting R^2 is 0.999, which shows an excellent fitting effect.

The process of model optimization

The coefficients belonged to the independent variables directly reflect their influence degree on the dependent variable. So, after sensitivity analysis the key influence factors in the frosting process will be found. Based on the factors obtained, the model optimization process is illustrated as the flowchart shown in Fig. 4, and the main steps of the process are listed as follows.

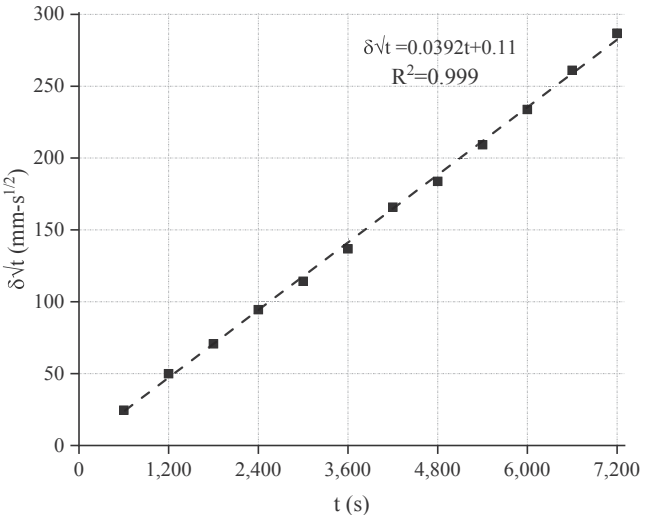

Fig. 3. Data sample with linear best fit.

i. Sensitivity analysis with independent and dependent variables corresponding to the experimental data is carried out;
ii. Combine the key factors obtained from sensitivity analysis with exhaustive method to generate groups of the optimized models to be verified;
iii. Take one of the optimized models to fit the corresponding experimental data, and output the value of the coefficients and *Cr*;
iv. Compare *Cr* of each group of the optimized models with that of other groups. If *Cr* of the new optimized model is bigger than

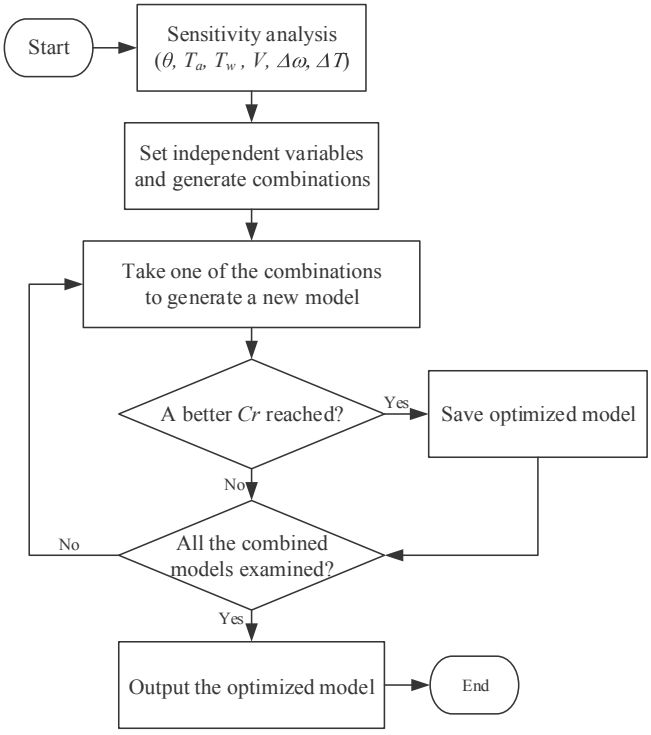

Fig. 4. Flowchart of optimizing the models in early frosting stage.

previous ones, save the model; if not, another new model will be selected for fitting;

v. Until all the combined optimized models have been fitted, the model with the best fitting effect, the maximum *Cr*, of all combinations including the theoretical model represented by Eq. (13) is output.

Results and discussions

Influence of each factor in the initial condition of frosting

According to the content of Section 2.3, after sensitivity analysis, the coefficients of the independent variables are obtained. Then sum up the absolute values of the coefficients, the proportions of each coefficient in the sum are shown in Fig. 5. It can be seen from Fig. 5(a) that, for the whole frosting process, the influence of ΔT is the largest, whose proportion reaches 45.29%, followed by T_w, $\Delta\omega$ and T_a, whose proportions are 23.1%, 20.97% and 9.73%, respectively. Moreover, the influence of V and θ can be almost ignored, because the sum of the proportions of these two factors is less than 1%. However, in order to show the influence of various factors in the initial conditions of the frosting process and modify part B accordingly, the core of the study is the influence of each factor on B. As shown in Fig. 5(b), with all the factors considered, the order of influence degree from large to small is $\Delta\omega$, ΔT, T_w, V, T_a, θ. Compared with the influence of the first three factors, that of the latter three is not obvious. That is, the proportions of $\Delta\omega$, ΔT and T_w are 39.42%, 35.58% and 21.15%, respectively, while the sum of the proportions of the latter three only reaches 3.84%. According to the results, with all the factors considered, $\Delta\omega$, ΔT and T_w are always the key factors influencing the frosting process. T_a is important for the whole frosting process, but not for the initial condition of frosting. V and θ seems to have little influence on frosting. Actually, as far as $\Delta\omega$ and ΔT are non-zero, the successive nucleation and embryo growth process will go on [31]. That means, $\Delta\omega$ and ΔT directly influence the mass driving potential. From the perspective of convective heat transfer, T_a and V will undoubtedly influence the frosting process, and higher temperature air usually can hold more moisture [25]. But for the frosting process on a cold plate which is dominated by the heat conduction, T_w mainly influences the heat transfer process, while the influence of T_a and V is not obvious. As mentioned earlier, the surface wettability has a strong influence on the no frost stage, as it affects the droplet crystallization process, while its influence disappears at latter frosting process.

Now review the part represented by b in Eq. (13), which is merely related to θ. According to the sensitivity analysis, it's known that θ actually has little influence on b. Therefore, such an expression of b can't reflect the initial conditions of frosting, which directly leads to the proportion of B/δ less than 1% within 1,200 s as shown in Table 1. As $\Delta\omega$, ΔT and T_w are the key influence factors on b among the factors considered, these three factors are taken as single, paired and triple combinations in the form of exhaustive method to investigate the effect of the optimized models on frosting.

The initial period of early frosting stage within 600 s

According to the flowchart in Fig. 4, the fitting results of each proposed model with 65 experimental data points within 600 s are shown in Table 2. It has been mentioned that the key influence factors on b are $\Delta\omega$, ΔT, T_w. However, *Cr* of the model obtained by the combination of these three factors in Group 7 is 75.38%, while *Cr* of the model obtained by the combination of $\Delta\omega$ and ΔT in Group 6 is 81.53%. Compared with the model under the interaction of three factors, the model under the interaction of $\Delta\omega$ and ΔT can better reflect the frosting process in the initial period of early frosting stage. And the heat conduction effect of cold plate on the growth of frost layer is not fully reflected at this period. The reason is, in this period, the frost thickness is small, thus the frost surface temperature is close to the cold plate temperature, maintaining at a lower temperature. At the same time, a lower frost surface temperature corresponds to a lower humidity of the saturated air, i.e. $\omega_{sat,w}$ [31]. Therefore, in this period, $\Delta\omega$ and ΔT are greater than the latter periods, and have greater mass driving potential to promote the nucleation and embryo growth process. And when the frost layer is initially formed, it will become an insulation and increase the heat transfer resistance owing to its porous characteristics, making the effect of T_w is not obvious at this period.

Above all, the new model for the initial period of the early frosting stage on the cold plate surface under forced convection conditions within 600 s is shown in Eq. (20), and the corresponding coefficient values are $c = 8449.6$, $m = 0.7983$, $n = 1.6827$, $c_1 = 0.5016$ and $c_2 = 1.5993$ with its $Cr = 81.53\%$.

$$\delta = c\left(\frac{\rho_a}{\rho_i}\right)\left(\frac{D\Delta\omega}{L}\right)Re^m Pr^{1/3} Ja^n \sqrt{t} + \frac{(\Delta\omega)^{c_1}(\Delta T)^{c_2}}{\sqrt{t}} \tag{20}$$

As shown in Table 2, the proportion of A/δ in Group 6 is from 70% to 100%, and the corresponding B/δ from 0 to 30%, which means the new model has reflected the proportion of early frosting stage within 600 s. Moreover, based on the theoretical model of Hermes et al. [8], a modified model proposed by same authors considering the important role of ΔT in the whole frosting process is introduced, as shown below.

$$\delta = m(\Delta T)^n \sqrt{t} + \frac{c_1 + c_2 \Delta T}{\sqrt{t}} \tag{21}$$

where, m, n, c_1 and c_2 are all constants. Compared with the theoretical

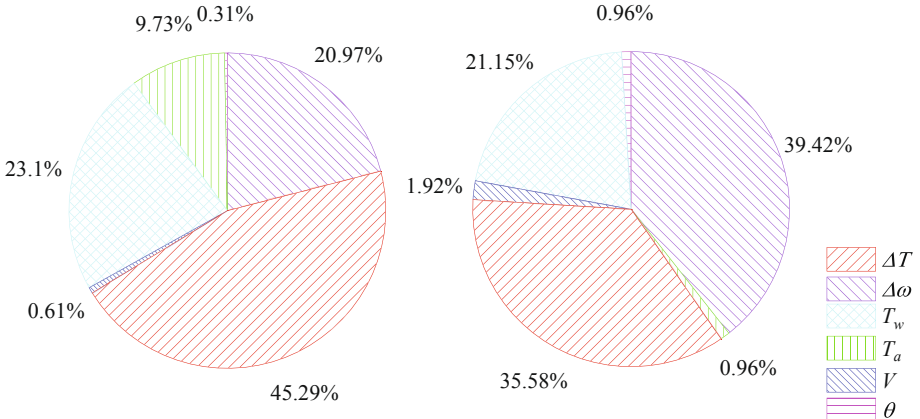

(a) Influence of each factor on a (b) Influence of each factor on b

Fig. 5. Sensitivity analysis of a and b with respect to $\Delta\omega$, ΔT, V, T_a, T_w, and θ.

Table 2
Results of each model in the initial period within 600 s.

Group	A	B	Coincidence number/Total number	Cr (%)	A/δ (%)	B/δ (%)
1	A_1 [a]	$\frac{(\Delta w)^c}{\sqrt{t}}$	48/65	73.84	>99	<1
2	A_1	$\frac{(\Delta T)^c}{\sqrt{t}}$	48/65	73.84	91 ~ 96	4 ~ 9
3	A_1	$\frac{(Tw)^c}{\sqrt{t}}$	48/65	73.84	91 ~ 96	4 ~ 9
4	A_1	$\frac{(\Delta T)^{c_1}(Tw)^{c_2}}{\sqrt{t}}$	46/65	70.76	4 ~ 20	80 ~ 96
5	A_1	$\frac{(\Delta w)^{c_1}(Tw)^{c_2}}{\sqrt{t}}$	47/65	72.30	26 ~ 69	31 ~ 74
6	A_1	$\frac{(\Delta w)^{c_1}(\Delta T)^{c_2}}{\sqrt{t}}$	53/65	81.53	70 ~ 100	0 ~ 30
7	A_1	$\frac{(\Delta w)^{c_1}(Tw)^{c_2}(\Delta T)^{c_3}}{\sqrt{t}}$	49/65	75.38	77 ~ 100	0 ~ 23
8	A_1	$\frac{de^{k\theta}}{\sqrt{t}}$	48/65	73.84	>99	<1
9	$m(\Delta T)^n\sqrt{t}$	$\frac{c_1+c_2\Delta T}{\sqrt{t}}$	40/65	61.54	85 ~ 290	−190 ~ 15

[a] $A_1 = c\left(\frac{\rho_a}{\rho_i}\right)\left(\frac{D\Delta\omega}{L}\right)Re^m Pr^{1/3} Ja^n\sqrt{t}$

model [8], Cr of the modified model for the whole frosting process is improved to 90%. However, when using this modified model to fit the experimental data points, which is shown in Group 9, its Cr only reaches 61.54%. And the proportion of A/δ of the modified model is even greater than 100%, correspondingly, the proportion of B/δ reaches a negative number. In other words, in order to reflect the growth of frost layer in the whole frosting process, the modified model has overemphasized the expression of A, which represents the whole frosting process, but the expression of B, which represents the early frosting stage, was ignored.

In the process of fitting with the theoretical and modified models of Hermes et al. [8] and the new model of this study, the ratio of A/δ under each selected data point within 600 s is shown in Fig. 6. It can be seen that A/δ of the frost model within 600 s represented by the theoretical model always adheres to 100%, which makes the B/δ representing the early stage insufficient. On the other hand, the modified model over-emphasizes the growth of frost layer in the whole frosting process, causing A/δ is even greater than 100%. However, the new model does not show excessive performance in A/δ, which makes B/δ reflect the proportion of fitting in the frosting process, thus increasing Cr.

To show the difference between this new model and previous models in the prediction of frost growth in the initial period of early frosting stage, a dimensionless model considering the frost surface temperature proposed by Hermes [30] and a simplified model on the surface of flat plate proposed by Sommers et al. [41] are introduced, as shown in Eqs. (22) and (23), respectively.

$$\begin{cases} X = \dfrac{\delta}{L} = \dfrac{\sqrt{d_1^2 + 4d_0\tau} - d_1}{2} \\ d_0 = \widetilde{\omega}\dfrac{\left(2+\widetilde{T}\right)}{\left(1+\widetilde{T}\right)(1+1/Ja)}, d_1 = \dfrac{\widetilde{k}}{Nu}\dfrac{\left(2+\widetilde{T}\right)}{\left(1+\widetilde{T}\right)(1+1/Ja)} \end{cases} \tag{22}$$

$$\delta = b_0 + b_1 \cdot t^{b_2} \tag{23}$$

where, X, $\widetilde{\omega}$, $\widetilde{T}$ and $\widetilde{k}$ are all dimensionless parameters, representing the dimensionless frost thickness, supersaturation degree, air-to-surface temperature difference and thermal conductivity, respectively. Nu is the Nusselt number associated with the boundary layer over the frost surface. b_0, b_1 and b_2 are constants related to the experimental conditions.

Compared with the experimental data proposed by Hermes et al. [8], prediction of the four models including the new model of this study, the modified model [8], the dimensionless model [30] and the simplified model [41] on the frost thickness in the initial period of early frosting stage is shown as Fig. 7. Take 15% as the allowable range of relative error deviation, as shown by the dotted line. Crs of the new model, the

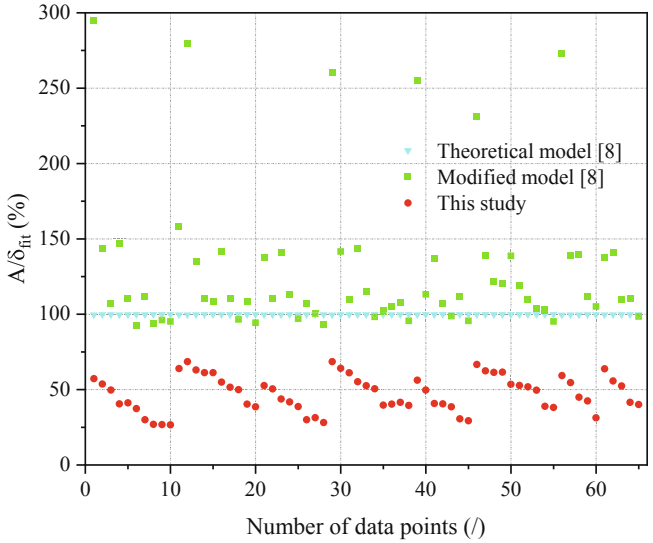

Fig. 6. Ratio of A/δ under each selected data point within 600 s.

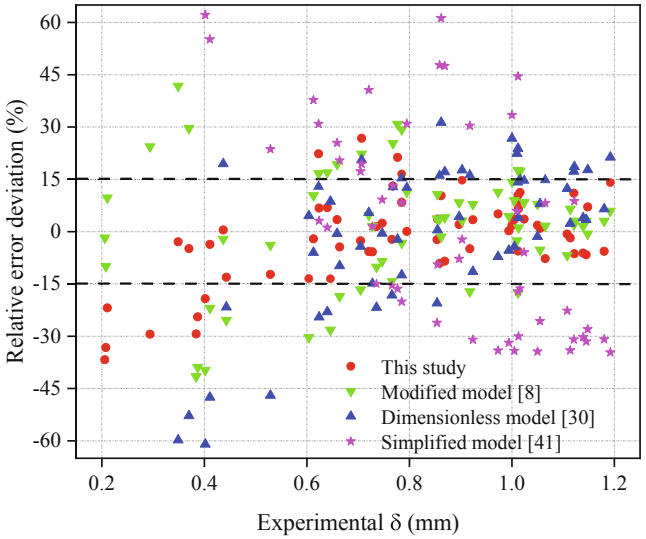

Fig. 7. Difference of relative error deviation between models within 600 s.

modified model, the dimensionless model and the simplified model are 81.53%, 61.54%, 49.23% and 21.53%, respectively.

Prediction effect of each model is clearly reflected in Fig. 7. It can be seen that the prediction of the simplified model is almost randomly distributed, which is caused by the random change of b_0, b_1 and b_2 due to the diversity of the experimental conditions. Moreover, when the frost thickness is 0.2–0.4 mm, the relative error deviation of the simplified model is greater than 60%, so it is not shown in the figure. After the frost thickness reaches 0.6 mm, prediction of frost thickness by the dimensionless model has been improved, while it's poor before 0.6 mm, which makes the relative error deviation present a left-down inclined distribution. Also, when the frost thickness is 0.2–0.4 mm, the relative error deviation of the dimensionless model is too large to be reflected. This is due to the fact that the early frosting stage is ignored in the dimensionless model. Compared with the other two models, relative error deviation of the modified model and the new model present a more uniformly middle distributed. And the new model is more in line with the requirements of relative error deviation than the modified model. And within the fitting range of frost layer thickness from 0.4 to 1.2 mm, the fitting relative error deviation of the new model is closer to 0 in the ordinate, which means the fitting effect can be better reflected.

It can be seen that there are no data points within 0–0.2 mm in Fig. 7. The reason is that, as shown in Fig. 1, there are frozen droplets in the no frost stage, which have a height of h. In the subsequent early frosting stage, the early frost layer will continue to grow on the frozen water droplet embryo, and the growth rate of frost layer along the vertical direction is fast. On the other hand, the experimental data obtained by Hermes et al. [8] is measured at 600 s, which means the frost layer has grown to a certain thickness.

The middle period of early frosting stage within 600–1,200 s

According to the flowchart in Fig. 4, the fitting results of each proposed model with 65 experimental data points within 600–1,200 s are shown in Table 3. As shown in Group 7, under the interaction of $\Delta\omega$, ΔT and T_w, Cr reaches the maximum value of 84.61%, which means the simultaneous action of these three factors can better reflect the frosting process during this period. As discussed earlier, the heat conduction effect of the cold plate on the growth of frost layer is not fully reflected within 600 s. Then, the results in Table 3 shows that the heat conduction effect of the cold plate is gradually fully reflected after 600 s. This result is enough to subvert our understanding of the key influence factors on the growth of frost layer from the very beginning, as it is generally reported that the heat conduction effect of cold plate on frosting must always account for a significant proportion in the whole frosting process. The reason is that the porous characteristics of the frost layer allows the moist air to get into and freeze inside the frost layer in the frosting process [31]. Afterwards, the frost layer becomes denser, correspondingly, the thermal conduction resistance decreases, resulting the heat conduction effect of cold plate increases. Actually, the growth of the frost layer will gradually reduce the heat conduction of the cold plate and increase the frost surface temperature, resulting in the decrease of $\Delta\omega$ and ΔT. But in this period, the frost surface still keeps at a low temperature, so the variation of $\Delta\omega$ and ΔT is not obvious.

Above all, the new model for the middle period of the early frosting stage on the cold plate surface under forced convection conditions within 600–1,200 s is shown in Eq. (24), and the corresponding coefficient values are $c = 9420533.9$, $m = 0.1669$, $n = 1.0336$, $c_1 = 156.4719$, $c_2 = 127.3022$, $c_3 = 9.7036$, with its $Cr = 84.61\%$.

$$\delta = c\left(\frac{\rho_a}{\rho_i}\right)\left(\frac{D\Delta\omega}{L}\right)Re^m Pr^{1/3} Ja^n\sqrt{t} + \frac{(\Delta\omega)^{c_1}(T_w)^{c_2}(\Delta T)^{c_3}}{\sqrt{t}} \tag{24}$$

Additionally, it can be seen from Group 7 that A/δ reaches 83% ~100%, correspondingly, B/δ is 0 ~ 17%. That means, compared with the proportion of B/δ in the initial period, the proportion of B/δ decreases significantly in the process of fitting within 600–1,200 s. The reason is that, B reflects the early frosting stage, the smaller the time is, the more the corresponding frosting process reflects the initial conditions. As time goes on, the specific proportion of B will gradually decrease, so the specific value of B/δ should also drop to a certain extent. On the other hand, when the modified model is used to express the frosting progress in the middle period of early frosting stage, there exists an over expression of A/δ, correspondingly, the proportion of B/δ even reaches a negative number, resulting in poor fitting of the frosting process.

Similarly, compare the four models including the model of this study, the modified model [8], the dimensionless model [30] and the simplified model [41] with the experimental data proposed by Hermes et al. [8] on the frost thickness in the middle period of early frosting stage, the relative error deviation of each model is shown as Fig. 8. Take 15% as the allowable range of relative error deviation, as shown by the dotted line. *Crs* of the new model, the modified model, the dimensionless model and the simplified model are 84.61%, 72.30%, 56.92% and 21.53%, respectively. That is, in the middle period of the early frosting stage, the new model, the modified model and the dimensionless model have improved the prediction of frost thickness, while the simplified model still has a poor performance. And it can be seen that the distribution of the relative error deviation of these four models is similar to that in the initial period, and the reason to the result is the same as illustrated above. Compared with the modified model, the relative error deviation of the new model is closer to the 0-axis. When the frost layer thickness is 1.0–1.8 mm, the new model has better fitting convergence effect, and

Table 3
Results of each model in the middle period within 600–1,200 s.

Group	A	B	Coincidence number/Total number	Cr (%)	A/δ (%)	B/δ (%)
1	A_1 [a]	$\frac{(\Delta w)^c}{\sqrt{t}}$	52/65	80.00	>99	<1
2	A_1	$\frac{(\Delta T)^c}{\sqrt{t}}$	52/65	80.00	3 ~ 23	77 ~ 97
3	A_1	$\frac{(Tw)^c}{\sqrt{t}}$	50/65	76.92	95 ~ 98	2 ~ 5
4	A_1	$\frac{(\Delta T)^{c_1}(Tw)^{c_2}}{\sqrt{t}}$	52/65	80.00	4 ~ 22	78 ~ 96
5	A_1	$\frac{(\Delta w)^{c_1}(Tw)^{c_2}}{\sqrt{t}}$	52/65	80.00	76 ~ 100	0 ~ 24
6	A_1	$\frac{(\Delta w)^{c_1}(\Delta T)^{c_2}}{\sqrt{t}}$	51/65	78.46	43 ~ 67	33 ~ 57
7	A_1	$\frac{(\Delta w)^{c_1}(Tw)^{c_2}(\Delta T)^{c_3}}{\sqrt{t}}$	55/65	84.61	83 ~ 100	0 ~ 17
8	A_1	$\frac{de^{k\theta}}{\sqrt{t}}$	51/65	78.46	>99	<1
9	$m(\Delta T)^n\sqrt{t}$	$\frac{c_1 + c_2\Delta T}{\sqrt{t}}$	47/65	72.30	95 ~ 150	−50 ~ 5

[a] $A_1 = c\left(\frac{\rho_a}{\rho_i}\right)\left(\frac{D\Delta\omega}{L}\right)Re^m Pr^{1/3} Ja^n\sqrt{t}$.

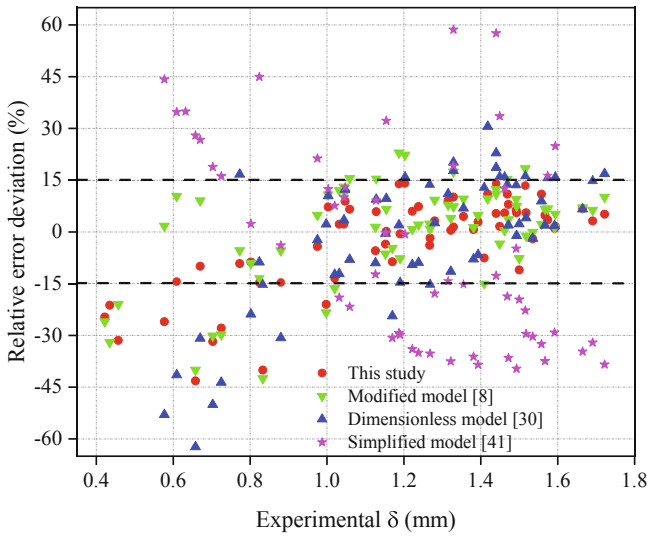

Fig. 8. Difference of relative error deviation between models within 600–1,200 s.

can make the fitting model and the experiment data present a better corresponding relationship.

The developed period of the early frosting stage within 1,200–2,400 s

According to the flowchart in Fig. 4, the fitting results of each model within 1,200–2,400 s are shown in Table 4. As shown in Group 5, the interaction of $\Delta\omega$ and T_w has a greater influence on the growth of frost layer in this period, with its *Cr* reaches 86.92%. From the previous discussions, the heat conduction effect of the cold plate surface begins to be fully reflected after 1,200 s. Then the period within 1,200–2,400 s examined here further confirms the previous conclusion. However, in the expression of B, ΔT was omitted, which means the effect of ΔT in the developed period was covered up by the interaction influence of the other two factors. As mentioned earlier, the growth of frost layer will lead to increase the frost surface temperature and the decrease of $\Delta\omega$ and ΔT. However, when the frost surface temperature increases by the same extent, the decrease of $\Delta\omega$ is smaller than that of ΔT [31]. That is, the influence of ΔT will decrease significantly at this period, while $\Delta\omega$ still has a certain influence on frosting.

Above all, the new model for the developed period of the early frosting stage on the cold plate surface under forced convection conditions within 1,200–2,400 s is shown in Eq. (25), and the corresponding coefficient values are $c = 5296776.8177$, $m = 0.2285$, $n = 1.0869$, $c_1 = 127.2331$, $c_2 = 149.4872$, with its $Cr = 86.92\%$.

$$\delta = c\left(\frac{\rho_a}{\rho_i}\right)\left(\frac{D\Delta w}{L}\right)Re^m Pr^{1/3} Ja^n\sqrt{t} + \frac{(\Delta\omega)^{c_1}(T_w)^{c_2}}{\sqrt{t}} \tag{25}$$

Additionally, as the frosting process goes on, the proportion of B in the developed period should be gradually reduced, which means it is no longer meaningful to deliberately increase the proportion of B/δ. As shown in Groups 8 and 9 in Table 4, the theoretical and the modified models [8] are used to express the frosting process within 1,200–2,400 s. Although the proportions of A/δ reach greater than 99%, correspondingly, the proportion of B/δ are less than 1%, *Crs* of these two models have exceeded *80%*. That is, in the middle and final frosting stages, optimization on the frosting model according to the expression of B won't help the fitting effect perform better. By contrast, optimizing the expression of A, which is mainly affected by ΔT, should be emphasized. The modified model [8] modifies A and B at the same time, but in fact, the core amendment is to modify the expression of A. So, the modified model can't reflect the frosting process well in the early frosting stage, while with the frosting process going on, *Cr* of the model is further improved.

The whole period of the early frosting stage within 2,400 s

According to the flowchart in Fig. 4, the fitting results of each model in the whole period of the early frosting stage within 2,400 s are shown in Table 5. As shown in Groups 5 and 7, *Crs* both reach 80%. It is reasonable to believe that the interaction of $\Delta\omega$ and T_w, or the simultaneous action of $\Delta\omega$, ΔT and T_w, have greater influence on the growth of frost layer in the whole period of the early frosting stage. However, when fitting the models during this period, 195 experimental data points are selected. Although such data points have reached a certain scale, with the increase of data points, the difference of fitting effect between these models will be further reflected. Therefore, one reason for the same *Crs* of Groups 5 and 7 is that the selected experimental data points are not enough to distinguish the fitting differences between these two models. On the other hand, from the analysis of Tables 2–4, $\Delta\omega$ and ΔT are the key factors in the initial and middle periods, while T_w is a key factor after the initial period and is further strengthened in the subsequent periods. Although the influence degree of each factor is different, which makes the frosting model change in each specific period, these three factors $\Delta\omega$, ΔT and T_w all play a key role in the initial and middle periods. So, for the evaluation of the frosting model within the whole period, the influence of three factors should be simultaneously considered.

Above all, the model for the whole period of the early frosting stage

Table 4
Results of each model in the developed period within 1,200–2,400 s.

Group	A	B	Coincidence number/Total number	*Cr* (%)	A/δ (%)	B/δ (%)
1	A_1 [a]	$\frac{(\Delta w)^c}{\sqrt{t}}$	109/130	83.84	>99	<1
2	A_1	$\frac{(\Delta T)^c}{\sqrt{t}}$	106/130	81.53	95 ~ 99	1 ~ 5
3	A_1	$\frac{(Tw)^c}{\sqrt{t}}$	106/130	81.53	95 ~ 99	1 ~ 5
4	A_1	$\frac{(\Delta T)^{c_1}(Tw)^{c_2}}{\sqrt{t}}$	106/130	81.53	95 ~ 99	1 ~ 5
5	A_1	$\frac{(\Delta w)^{c_1}(Tw)^{c_2}}{\sqrt{t}}$	113/130	86.92	75 ~ 100	0 ~ 25
6	A_1	$\frac{(\Delta w)^{c_1}(\Delta T)^{c_2}}{\sqrt{t}}$	102/130	78.46	>99	<1
7	A_1	$\frac{(\Delta w)^{c_1}(Tw)^{c_2}(\Delta T)^{c_3}}{\sqrt{t}}$	102/130	78.46	67 ~ 100	0 ~ 33
8	A_1	$\frac{de^{k\theta}}{\sqrt{t}}$	108/130	83.07	>99	<1
9	$m(\Delta T)^n\sqrt{t}$	$\frac{c_1 + c_2\Delta T}{\sqrt{t}}$	104/130	80.00	>99	<1

[a] $A_1 = c\left(\frac{\rho_a}{\rho_i}\right)\left(\frac{D\Delta\omega}{L}\right)Re^m Pr^{1/3} Ja^n\sqrt{t}$.

Table 5
Results of each model in the whole early frosting stage within 2,400 s.

Group	A	B	Coincidence number/Total number	Cr (%)	A/δ (%)	B/δ (%)
1	A_1[a]	$\frac{(\Delta w)^c}{\sqrt{t}}$	152/195	77.94	>99	<1
2	A_1	$\frac{(\Delta T)^c}{\sqrt{t}}$	145/195	74.35	91 ~ 98	2 ~ 9
3	A_1	$\frac{(Tw)^c}{\sqrt{t}}$	145/195	74.35	91 ~ 98	2 ~ 9
4	A_1	$\frac{(\Delta T)^{c_1}(Tw)^{c_2}}{\sqrt{t}}$	145/195	74.35	91 ~ 98	2 ~ 9
5	A_1	$\frac{(\Delta w)^{c_1}(Tw)^{c_2}}{\sqrt{t}}$	156/195	80.00	70 ~ 100	0 ~ 30
6	A_1	$\frac{(\Delta w)^{c_1}(\Delta T)^{c_2}}{\sqrt{t}}$	153/195	78.46	76 ~ 99	1 ~ 24
7	A_1	$\frac{(\Delta w)^{c_1}(Tw)^{c_2}(\Delta T)^{c_3}}{\sqrt{t}}$	156/195	80.00	73 ~ 100	0 ~ 27
8	A_1	$\frac{de^{k\theta}}{\sqrt{t}}$	151/195	77.43	>99	<1
9	$m(\Delta T)^n\sqrt{t}$	$\frac{c_1+c_2\Delta T}{\sqrt{t}}$	145/195	74.35	>99	<1

[a] $A_1 = c\left(\frac{\rho_a}{\rho_i}\right)\left(\frac{D\Delta\omega}{L}\right)Re^m Pr^{1/3} Ja^n\sqrt{t}$.

on the cold plate surface under forced convection conditions is shown in Eq. (26), and the corresponding coefficient values are $c = 7696971.25$, $m = 0.1889$, $n = 1.0536$, $c_1 = 122.5853$, $c_2 = 104.3204$, $c_3 = 0.00008$ with its $Cr = 80\%$.

$$\delta = c\left(\frac{\rho_a}{\rho_i}\right)\left(\frac{D\Delta\omega}{L}\right)Re^m Pr^{1/3} Ja^n\sqrt{t} + \frac{(\Delta\omega)^{c_1}(T_w)^{c_2}(\Delta T)^{c_3}}{\sqrt{t}} \quad (26)$$

Moreover, as shown in Period 2,400② in Table 6, Eq. (26) is used to fit the frosting process at 2,400 s with its Cr reaches 92.30%, which means that Eq. (26) can greatly reflect the frosting process after 1,200 s.

Improvement of the new models in different periods within 2,400 s

The results of comparison between the modified model [8] and the new models of this study within 2,400 s is shown in Table 6. It is worth mentioning that the dimensionless model [30] and the simplified model [41] do not reflect the consideration of the initial conditions of frosting, and Crs of these two models for the early frosting stage is poor, so they are not included in the comparison.

It can be seen from Table 6 that in the early frosting stage, the new models show obvious optimization effect when compared with the modified model, especially in the initial period within 0–600 s as shown in Group 1, with its fitting improvement rate reaches 32.5%. B represents the initial conditions of frosting, so in the early frosting stage, emphasis should be placed on the proportion of B, as shown in Group 1, the proportion of B/δ is from 34% to 74%. As the frosting process goes on, the proportion of B in the overall expression also has a significant decline, so the optimization effect of the new models for B has a certain decline. As shown in Groups 2 and 5, which represent the middle and developed periods of the early frosting stage, the improvement rates of the new models are 17.02% and 7.63%, respectively.

Although the increase range is not as good as that in the initial period, it is enough to show that the proportion of B in each model should be paid attention to in the early frosting stage. Therefore, the expression of the new model for B can significantly reflect the growth of frost layer in the frosting process. Additionally, in the model optimization which involves the time close to 2,400 s, in the Groups 3 and 4, the difference of fitting effect between the new model and the modified model is small. The reason is that the reflection of B in the whole frosting model is no longer important in the developed early and non-early

Table 6
Comparison between the modified and optimized models in each period within 2,400 s.

Group	Period (s)	The modified model of Hermes et al. [8]				The new models				Comparison
		Model	Cr (%)	A/δ (%)	B/δ (%)	Model	Cr (%)	A/δ (%)	B/δ (%)	Improvement rate (%)
1	0–600	$m(\Delta T)^n\sqrt{t} + \frac{c_1+c_2\Delta T}{\sqrt{t}}$	61.53	85 ~ 290	−190 ~ 15	$c\left(\frac{\rho_a}{\rho_i}\right)\left(\frac{D\Delta w}{L}\right)\mathrm{Re}^m Pr^{1/3} Ja^n\sqrt{t} + \frac{(\Delta w)^{c_1}(\Delta T)^{c_2}}{\sqrt{t}}$	81.53	26 ~ 66	34 ~ 74	32.50
2	600–1,200	$m(\Delta T)^n\sqrt{t} + \frac{c_1+c_2\Delta T}{\sqrt{t}}$	72.30	95 ~ 150	−50 ~ 5	$c\left(\frac{\rho_a}{\rho_i}\right)\left(\frac{D\Delta w}{L}\right)\mathrm{Re}^m Pr^{1/3} Ja^n\sqrt{t} + \frac{(\Delta w)^{c_1}(\Delta T)^{c_2}(Tw)^{c_3}}{\sqrt{t}}$	84.61	43 ~ 66	34 ~ 57	17.02
3	2,400①	$m(\Delta T)^n\sqrt{t} + \frac{c_1+c_2\Delta T}{\sqrt{t}}$	87.69	97 ~ 120	−20 ~ 3	$c\left(\frac{\rho_a}{\rho_i}\right)\left(\frac{D\Delta w}{L}\right)\mathrm{Re}^m Pr^{1/3} Ja^n\sqrt{t} + \frac{de^{k\theta}}{\sqrt{t}}$	92.30	97 ~ 99	1 ~ 3	5.25
4	2,400②	$m(\Delta T)^n\sqrt{t} + \frac{c_1+c_2\Delta T}{\sqrt{t}}$	87.69	97 ~ 120	−20 ~ 3	$c\left(\frac{\rho_a}{\rho_i}\right)\left(\frac{D\Delta w}{L}\right)\mathrm{Re}^m Pr^{1/3} Ja^n\sqrt{t} + \frac{(\Delta w)^{c_1}(\Delta T)^{c_2}(Tw)^{c_3}}{\sqrt{t}}$	92.30	86 ~ 100	0 ~ 14	5.25
5	1,200–2,400	$m(\Delta T)^n\sqrt{t} + \frac{c_1+c_2\Delta T}{\sqrt{t}}$	80.76	95 ~ 150	−50 ~ 5	$c\left(\frac{\rho_a}{\rho_i}\right)\left(\frac{D\Delta w}{L}\right)\mathrm{Re}^m Pr^{1/3} Ja^n\sqrt{t} + \frac{(\Delta w)^{c_1}(Tw)^{c_2}}{\sqrt{t}}$	86.92	75 ~ 100	0 ~ 25	7.63
6	0–2,400	$m(\Delta T)^n\sqrt{t} + \frac{c_1+c_2\Delta T}{\sqrt{t}}$	74.35	80 ~ 290	−190 ~ 20	$c\left(\frac{\rho_a}{\rho_i}\right)\left(\frac{D\Delta w}{L}\right)\mathrm{Re}^m Pr^{1/3} Ja^n\sqrt{t} + \frac{(\Delta w)^{c_1}(\Delta T)^{c_2}(Tw)^{c_3}}{\sqrt{t}}$	80.00	82 ~ 100	0 ~ 18	7.50

frosting stages after 1,200 s, so the investigation of A is more reasonable.

Comparison between the experimental and fitted frost thickness with the new models of this study, modified model [8], dimensionless model [30] and simplified model [41] within 1,200 s is shown in Fig. 9. The two straight lines represent the allowable range of relative error deviation of 15% between the experimental and fitted data. It can be seen that the simplified model and the dimensionless model have a serious deviation within 1200 s. The fitting effect of the modified model is improved when the frost thickness is greater than 0.6 mm, however, in the fitting of frost thickness within 0.2–0.6 mm, the fitting effect is insufficient. The reason is that the frost thickness of this value represents the growth of frost layer in the initial period of the early frosting stage. In addition to the large deviation for several values, the new model has good fitting effect in the whole 1,200 s, and distribution of fitting points is more concentrated.

The whole frosting process within 7,200 s is described by the models shown in Table 7. It can be seen that the proportion of A/δ is gradually increasing in the early frosting stage, correspondingly, that of B/δ decreasing, which means the proportion reflecting the initial conditions of frosting should decrease. In the subsequent frosting stages, the theoretical model of **Eq. (13)** is used to reflect the frosting process in each period, because the model could reflect the frosting process well. That is, from the specific proportion value of A/δ and B/δ, i.e. A/δ is from 65% to 96% and B/δ is from 4% to 35% in Groups 4–6, the theoretical model has representation of A and B, resulting in Crs reach at least 90%. The comparison between the experimental and fitted frost thickness within 7,200 with the models in Table 7 is shown in Fig. 10. The two straight lines represent the allowable range of relative error deviation of 15% between the experimental and fitted data points. It can be seen that most of the data points conform to the fitting error range. After this correction process, the overall Cr of the frosting models within 7,200 s is 90.35%, which is 8.86% higher than previous theoretical model of Hermes et al. [8].

Model validation

To verify whether the new models can better reflect the early frosting process under different working conditions, the experimental data obtained from Cheng and Wu [42] and Lai et al. [43] based on the conditions of cold plate and round tube, respectively, is used. Because this study mainly focuses on optimizing the initial conditions of frosting, optimization of the expression of A in the modified model proposed by Hermes et al. [8] is considered. Result shows that the frosting model with simultaneously optimized expressions of A and B improved the reflection of the early frosting process compared with the previous modified and new models with single optimized expression, and the average improvement rate reaches 11.82%. The combined optimized models used for the initial, middle and developed periods of the early frosting stage are shown in Eqs. (27)–(29), respectively.

$$\delta = m(\Delta T)^n\sqrt{t} + \frac{(\Delta\omega)^{c_1}(\Delta T)^{c_2}}{\sqrt{t}} \tag{27}$$

$$\delta = m(\Delta T)^n\sqrt{t} + \frac{(\Delta\omega)^{c_1}(T_w)^{c_2}}{\sqrt{t}} \tag{28}$$

$$\delta = m(\Delta T)^n\sqrt{t} + \frac{(\Delta\omega)^{c_1}(T_w)^{c_2}(\Delta T)^{c_3}}{\sqrt{t}} \tag{29}$$

The results of the models compared with the experimental data of early frosting stage under different working conditions are listed in Table 8. It can be seen that although the frosting process is complicated under different conditions, the expressions of the models could show the corresponding period of frosting process well. As the frosting condition of this study is the early frosting process on cold plate, the fitting effect of experimental data on cold plate from Cheng and Wu [42] is good, whose error deviation rate is generally controlled within 5%. On the other hand, when introducing the experimental data on round tube from Lai et al. [43], although it shows a large error offset in the initial period, whose error deviation rate reaches 17.48% as shown in Case 4, the fitting effect is gradually improved in the subsequent periods. The reason is that the difference of the shape between the cold plate and the tube will inevitably lead to the difference of heat transfer process. However, with the development of frosting, the frosting process tends to be stable and ΔT becomes the most vital factor affecting the frosting process. The influence of ΔT conceals other factors on frosting, with geometric differences included. In the fitting of the early, middle and developed periods of the early frosting stages, the average error migration rates of each period are 7.4%, 5.93% and 3.31%, respectively. Such average migration rates illustrate the good fitting effect of the corresponding optimized models for each period in early frosting stage.

It should be noted that there is a smaller deviation in the initial period of Case 6, which is only 2.69%. This is because the measurement deviation of frost thickness in the experiment always exists. In the early frosting stage, the frost thickness is small, thus minor measurement deviation may also have a great impact on the fitting process. However, when using the model to fit and analyze the experimental data, the originality of the experimental data should be fully considered. Therefore, in the fitting process, the fitting results of each point are the final content that should be reflected. But in fact, based on the trend of current fitting results, the deviation of the initial period of Case 6 should be at least>10%.

Comparisons between experimental and fitted frost thickness on cold plate and round tube in the early frosting stage are shown as Figs. 11 and 12. It can be seen from Fig. 11 that the fitted frost thickness is always close to the experimental frost thickness with the increase of time. And as the frosting process goes on, the relative error deviation gradually converges to the 0-axis, which means the fitting effect is improving. As shown in Fig. 12, there is a significant gap between the experimental and fitted frost thickness from the beginning. However, as the frosting process goes on, the relative error deviation quickly converges to the 0-axis, and the fitting effect has improved a lot at the end of the developed period of the early frosting stage.

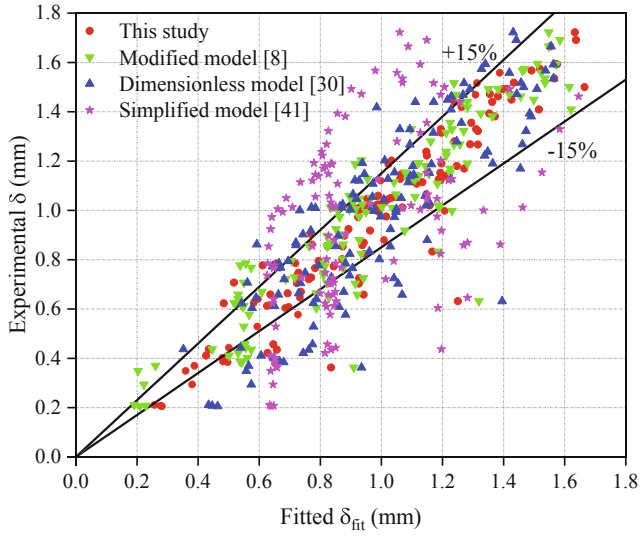

Fig. 9. Comparison between experimental and fitted frost thickness within 1,200 s.

Conclusions

New frosting models under forced convection conditions are developed and validated, with surface and environmental factors considered. To improve the models' accuracy, the early frosting stage is specially

Table 7
Summary of the final models selected in each period within 7,200 s.

Group	Period (s)	Model	Coincidence number/Total number	*Cr* (%)	*A*/*δ* (%)	*B*/*δ* (%)
1	600	$c\left(\frac{\rho_a}{\rho_i}\right)\left(\frac{D\Delta w}{L}\right)\mathrm{Re}^m Pr^{1/3} Ja^n\sqrt{t}+\frac{(\Delta w)^{c_1}(\Delta T)^{c_2}}{\sqrt{t}}$	53/65	81.53	26 ~ 69	31 ~ 74
2	1,200	$c\left(\frac{\rho_a}{\rho_i}\right)\left(\frac{D\Delta w}{L}\right)\mathrm{Re}^m Pr^{1/3} Ja^n\sqrt{t}+\frac{(\Delta w)^{c_1}(\Delta T)^{c_2}(Tw)^{c_3}}{\sqrt{t}}$	55/65	84.61	83 ~ 100	0 ~ 17
3	2,400	$c\left(\frac{\rho_a}{\rho_i}\right)\left(\frac{D\Delta w}{L}\right)\mathrm{Re}^m Pr^{1/3} Ja^n\sqrt{t}+\frac{(\Delta w)^{c_1}(\Delta T)^{c_2}(Tw)^{c_3}}{\sqrt{t}}$	60/65	92.30	97 ~ 99	1 ~ 3
4	3,000–4,200	$c\left(\frac{\rho_a}{\rho_i}\right)\left(\frac{D\Delta w}{L}\right)\mathrm{Re}^m Pr^{1/3} Ja^n\sqrt{t}+\frac{de^{k\vartheta}}{\sqrt{t}}$	177/195	90.76	90 ~ 96	4 ~ 10
5	4,800–6,000	$c\left(\frac{\rho_a}{\rho_i}\right)\left(\frac{D\Delta w}{L}\right)\mathrm{Re}^m Pr^{1/3} Ja^n\sqrt{t}+\frac{de^{k\vartheta}}{\sqrt{t}}$	179/195	91.79	72 ~ 88	12 ~ 28
6	6,600–7,200	$c\left(\frac{\rho_a}{\rho_i}\right)\left(\frac{D\Delta w}{L}\right)\mathrm{Re}^m Pr^{1/3} Ja^n\sqrt{t}+\frac{de^{k\vartheta}}{\sqrt{t}}$	122/130	93.84	65 ~ 83	17 ~ 35

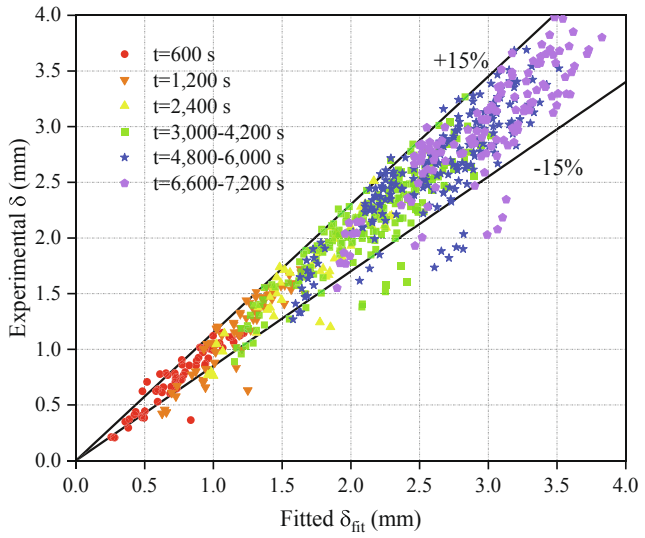

Fig. 10. Comparison between experimental and fitted frost thickness within 7,200 s.

analyzed, and initial, middle and developed periods of early frosting stage are proposed in this study. The following conclusions could be summarized.

a) Sensitivity analysis with surface and environmental factors considered shows that $\Delta\omega$, ΔT and T_w are the key factors influencing the frosting process. Proportions of these three factors for the early frosting stage reach 39.42%, 35.58% and 21.15%, respectively.
b) New models with emphasis on the initial conditions of the frosting process are developed. *Crs* of the new models reach 90.35% for the whole frosting process and 83% for the early frosting stage, which are increased by at least 8.86% and 15.28% than previous models, respectively.
c) In the initial period of the early frosting, the interaction of $\Delta\omega$ and ΔT mostly reflect the frosting process, while the heat conduction effect of the cold plate is not fully reflected. *Cr* of the new model considering the important role of $\Delta\omega$ and ΔT reaches 81.53%, which is increased by 10.41%~32.48% than previous models.
d) In the middle period of the early frosting stage, $\Delta\omega$, ΔT and T_w simultaneously have important influence on the frosting process, which means the heat conduction effect of the cold plate is gradually fully reflected at this period. *Cr* of the new model simultaneously considering the important role of $\Delta\omega$, ΔT and T_w reaches 84.61%, which is increased by 7.84%~17.03% than previous models.
e) In the developed period of the early frosting stage, the interaction of $\Delta\omega$ and T_w mostly reflects the frosting process. That means, the heat conduction effect of the cold plate is fully reflected, while the effect of ΔT was covered up. *Cr* of the new model considering the important role of $\Delta\omega$, and T_w reaches 86.92%, which is increased by 7.63% than previous models.

CRediT authorship contribution statement

Lei Shangwen: Methodology. **Song Mengjie:** . **Pekař Libor:** . **Shen Jun:** .

Declaration of Competing Interest

The authors declare that they have no known competing financial

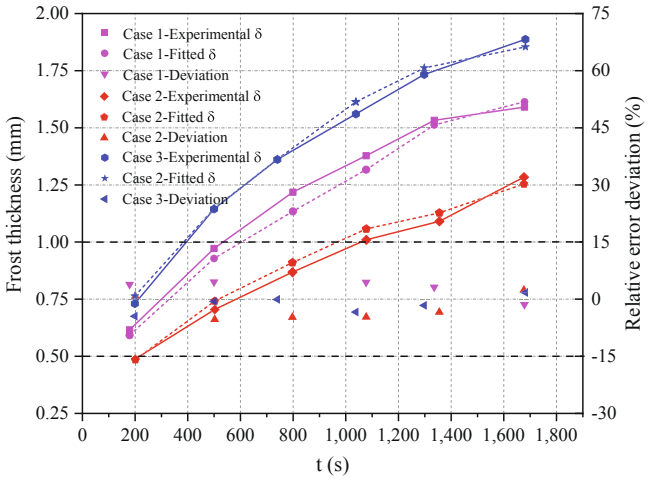

Fig. 11. Comparison between experimental and fitted frost thickness on cold plate.

Table 8
Model validation on the conditions of cold plate and round tube.

Period	Deviation (%)						Max Deviation (%)	Mean Deviation (%)
	Case 1	Case 2	Case 3	Case 4	Case 5	Case 6		
Initial	4.16	3.06	2.56	17.48	14.45	2.69	17.48	7.40
Middle	5.65	4.75	1.74	7.51	12	3.93	12	5.93
Developed	1.41	2.92	4.24	5.02	6.43	2.41	6.43	3.31

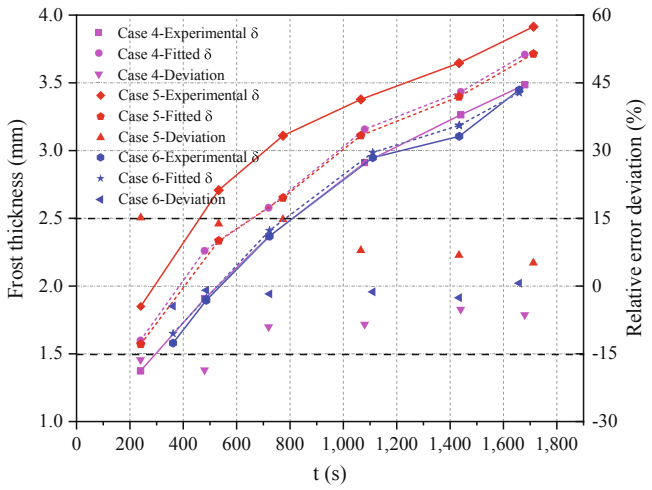

Fig. 12. Comparison between experimental and fitted frost thickness on round tube.

interests or personal relationships that could have appeared to influence the work reported in this paper.

Acknowledgments

The corresponding author acknowledges the financial supports from the National Natural Science Foundation of China (No. 52076013, 51925605), Beijing Municipal Science & Technology Commission (No. 3212024), Discovery Early Career Researcher Award (DECRA) 2020, Australian Research Council, Australia (No. DE200101747), Open Fund of Key Laboratory of Icing and Anti/De-icing (Grant No. IADL20200104), the CAS Key Laboratory of Cryogenics, Technical Institute of Physics and Chemistry, China (No. CRYO202001), and Chinese Association of Refrigeration (No. CAR20-04).

References

[1] Lee YB, Ro ST. Frost formation on a vertical plate in simultaneously developing flow. Exp Therm Fluid Sci 2002;26(8):939–45.
[2] Huang L, Liu Z, Liu Y, Gou Y, Wang J. Experimental study on frost release on fin-and-tube heat exchangers by use of a novel anti-frosting paint. Exp Therm Fluid Sci 2009;33(7):1049–54.
[3] Liu Z, Wang H, Zhang X, Meng S, Ma C. An experimental study on minimizing frost deposition on a cold surface under natural convection conditions by use of a novel anti-frosting paint. Part I. Anti-frosting performance and comparison with the uncoated metallic surface. Int J Refrig 2006;29(2):229–36.
[4] Song MJ, Mao N, Xu YJ, Deng SM. Challenges in, and the development of, building energy saving techniques, illustrated with example of an air source heat pump. Therm Sci Eng Prog 2019;10:337–56.
[5] Nath S, Ahmadi SF, Boreyko JB. A review of condensation frosting. Nanosc Microsc Therm 2017;21(2):81–101.
[6] Song M, Deng S, Dang C, Mao N, Wang Z. Review on improvement for air source heat pump units during frosting and defrosting. Appl Energy 2018;211:1150–70.
[7] Song MJ, Dang CB, Higashi T, Hihara E. Review of experimental data associated with the solidification characteristics of water droplets on a cold plate surface at the early frosting stage. Energ Build 2020;223:110103.
[8] Hermes CJL, Nascimento VS, Loyola FR, Cardoso RP, Sommers AD. A study of frost build-up on hydrophilic and hydrophobic surfaces under forced convection conditions. Exp Therm Fluid Sci 2019;100:76–88.
[9] Song M, Dang C. Review on the measurement and calculation of frost characteristics. Int J Heat Mass Transf 2018;124:586–614.
[10] Wang Z-J, Kwon D-J, Lawrence DeVries K, Park J-M. Frost formation and anti-icing performance of a hydrophobic coating on aluminum. Exp Therm Fluid Sci 2015;60:132–7.
[11] Amer M, Wang CC. Experimental investigation on defrosting of a cold plate via ultrasonic vibration under nature convection. Appl Therm Eng 2020;179:115729.
[12] Lüer A, Beer H. Frost deposition in a parallel plate channel under laminar flow conditions. Int J Therm Sci 2000;39(1):85–95.
[13] Sheikholeslami M, Jafaryar M, Said Z, Alsabery AI, Babazadeh H, Shafee A. Modification for helical turbulator to augment heat transfer behavior of nanomaterial via numerical approach. Appl Therm Eng 2021;182:115935.
[14] Sheikholeslami M, Jafaryar M, Abohamzeh E, Shafee A, Babazadeh H. Energy and entropy evaluation and two-phase simulation of nanoparticles within a solar unit with impose of new turbulator. Sustain Energy Technol 2020;39:100727.
[15] Zhang T, O'Neal DL, McClain ST. Analysis of frost thickness and roughness growth from the perspective of frost crystal structure. Int J Refrig 2020;112:314–23.
[16] Hosseini SH, Valizadeh M, Zendehboudi A, Song MJ. General correlations for frost thermal conductivity on parallel surface channels. Energ Build 2020;225:110282.
[17] Léoni A, Mondot M, Durier F, Revellin R, Haberschill P. State-of-the-art review of frost deposition on flat surfaces. Int J Refrig 2016;68:198–217.
[18] Mao N, Hao JY, He TB, Xu YJ, Song MJ, Tang JF. Unsteady heat transfer properties of spray falling over a horizontal tube in an oily sewage source heat pump. Appl Therm Eng 2020;179:115675.
[19] Lee M-Y, Kim Y, Lee D-Y. Experimental study on frost height of round plate fin-tube heat exchangers for mobile heat pumps. Energies 2012;5(9):3479–91.
[20] Wu XM, Hu S, Chu FQ. Experimental study of frost formation on clod surfaces with various fin layouts. Appl Therm Eng 2016;95:95–105.
[21] Armengol JM, Salinas CT, Xaman J, Ismail KAR. Modeling of frost formation over parallel cold plates considering a two-dimensional growth rate. Int J Therm Sci 2016;104:245–56.
[22] Zhuang D, Yang Y, Ding G, Zhan F. Optimization of fin surface wettability for promoting the dust removal in heat exchangers under frosting-defrosting conditions. Int J Refrig 2020;109:143–53.
[23] Zuo Z, Liao R, Zhao X, Song X, Qiao Z, Guo C, et al. Anti-frosting performance of superhydrophobic surface with ZnO nanorods. Appl Therm Eng 2017;110:39–48.
[24] Antonini C, Innocenti M, Horn T, Marengo M, Amirfazli A. Understanding the effect of superhydrophobic coatings on energy reduction in anti-icing systems. Cold Reg Sci Technol 2011;67(1-2):58–67.
[25] Sommers AD, Gebhart CW, Hermes CJL. The role of surface wettability on natural convection frosting: Frosting growth data and a new correlation for hydrophilic and hydrophobic surfaces. Int J Heat Mass Transf 2018;122:78–88.
[26] Lee J, Lee K-S. The behavior of frost layer growth under conditions favorable for desublimation. Int J Heat Mass Transf 2018;120:259–66.
[27] Lee H, Shin J, Ha S, Choi B, Lee J. Frost formation on a plate with different surface hydrophilicity. Int J Heat Mass Transf 2004;47:4881–93.
[28] Kim M-H, Kim H, Lee K-S, Kim DR. Frosting characteristics on hydrophobic and superhydrophobic surfaces: a review. Energy Convers Manage 2017;138:1–11.
[29] Sheng W, Liu PP, Dang CB, Liu GX. Review of restraint frost method on the cold surface. Renew Sustain Energy Rev 2017;79:806–13.
[30] Hermes CJL. An analytical solution to the problem of frost growth and densification on flat surfaces. Int J Heat Mass Transfers 2012;55(23-24):7346–51.
[31] Hermes CJL, Piucco RO, Barbosa JR, Melo C. A study of frost growth and densification on flat surfaces. Exp Therm Fluid Sci 2009;33(2):371–9.
[32] Kim D, Kim C, Lee K-S. Frosting model for predicting macroscopic and local frost behaviors on a cold plate. Int J Heat Mass Transfer 2015;82:135–42.
[33] Negrelli S, Hermes CJL. A simi-empirical correlation for the thermal conductivity of frost. Int J Refrig 2015;58:243–52.
[34] Zendehboudi A, Hosseini SH. Modeling of the frost deposition by natural convection on horizontal ultra-low-temperature surfaces. J Therm Anal Calorim 2019;137(6):2029–43.
[35] Song M, Liu S, Deng S, Sun Z, Yan H. Experimental investigation on reverse cycle defrosting performance improvement for an ASHP unit by evenly adjusting the refrigerant distribution in its outdoor coil. Appl Therm Eng 2017;114:611–20.
[36] Seyyed HH, Valizadeh M, Zendehboudi A, Song MJ. General correlations for frost thermal conductivity on parallel surface channels. Energy Build 2020;225:110282.
[37] Halaby A, Ghoneim W, Helal A. Sensitivity analysis and comparative studies for energy sustainability in sewage treatment. Sustain Energy Technol 2017;19:42–50.
[38] Leoni A, Mondot M, Durier F, Revellin R, Haberschill P. Frost formation and development on flat plate: experimental investigation and comparison to predictive methods. Exp Therm Fluid Sci 2017;88:220–33.
[39] Cheng CH, Cheng YC. Prediction of frost growth on a cold plate in atmospheric air. Int Commun Heat Mass Transfer 2001;28:953–62.
[40] Hermes CJL, Loyola FR, Nascimento VS. A semi-empirical correlation for the frost density. Int J Refrig 2014;46:100–4.
[41] Sommers AD, Truster NL, Napora AC, Riechman AC, Caraballo EJ. Densification of frost on hydrophilic and hydrophobic substrates- examining the effect of surface wettability. Exp Therm Fluid Sci 2016;75:25–34.
[42] Cheng CH, Wu KH. Observation of early-stage frost formation on a cold plate in atmospheric air flow. J Heat Trans-T ASME 2003;125:95–102.
[43] Lai TW, Ding P, Dong XJ, Zhang BL, Chen XZ, Hou Y. Experimental study on the frosting characteristics of round tube in confined circular flow path at low temperature. Appl Therm Energy 2020;171:115075.